# Hardware-assisted Direction Estimation for Mobile Robot Target Tracking Applications

Geunho Lee
Dept. of Environmental Robotics
University of Miyazaki
1-1 Gakuen Kibanadai-nishi, Miyazaki 889-2192, Japan
Email: geunho@cc.miyazaki-u.ac.jp

Kazutaka Tatara and Nak Young Chong
School of Information Science
Japan Advanced Institute of Science and Technology (JAIST)
1-1 Asahidai, Nomi, Ishikawa 923-1292, Japan
Email: {k_tatara, nakyoung}@jaist.ac.jp

***Abstract*—This paper addresses design and implementation issues for the directional sensing of electromagnetic waves, aiming to provide an efficient solution to mobile robot target tracking for various applications. What is the most important aspect from the practical point of view is how to realize accurate measurements of the bearing to the transponder(s). For the purpose, a novel direction-of-arrival (DoA) estimation model is proposed using a minimum number of antennas. Another focus lies in the implementation of an in-house DoA detector prototype considering the simplicity and generality of hardware configurations. This paper explains details of a purpose-built, cost-efficient solution ranging from the estimation model design to its hardware implementation suitable for autonomous robot navigation. Experimental results show that the proposed method for DoA estimation and its hardware prototype can be considered quite satisfactory in a normal office environment.**

## I. Introduction

With recent advances in robotic technologies, diverse mobile robots have been deployed into our homes, public places, and even outer space. Despite their expanded lineup that looks promising, the fundamental challenge to autonomous navigation still remains in unstructured and cluttered environments. For example, a wide variety of tasks await autonomous mobile robots, such as searching for survivors in mountainous districts, clearing snow along streets, and monitoring wild animals. The one thing those tasks have in common is regarded as a target-oriented mission where robots approach a reference while being oriented toward its direction. Moreover, the tasks would likely be performed in environments with uncertain geographic and poor weather conditions. With these considerations in mind, we aim to develop a direction-sensing system capable of communication, enabling the widespread use of transponders for mobile robot target tracking missions.

Advances in wireless communication technologies have made it possible to design and develop a wide variety of electromagnetic signal based measurement systems. Such technological achievements allow us to obtain bearing or range information by analyzing signal properties such as strength, frequency, and phase. Practically, the electromagnetic signal based system enables robots to use their antenna units for wireless communication links. This could yield a simple and compact hardware configuration, without requiring any of various types of position sensors. Compared with cameras and proximity sensors, the electromagnetic signal based sensors do not require lines of sight in the cluttered environment. Typical measurement technologies include received signal strength (RSS) [1], [2], direction of arrival (DoA) [3]-[5], time of arrival (ToA) [6], [7], time difference of arrival (TDoA) [8], [9], and frequency difference of arrival (FDoA) [10], [11]. Specifically, the features of the DoA technology can be summarized as follow: 1) robustness against changes in the output power of an electromagnetic source, 2) general hardware configuration without sophisticated devices such as global timer and antenna angle controlling unit, and 3) computational tractability avoiding unnecessary details, and 4) extra information encoded in electromagnetic waves.

Among technologies required for the aforementioned robot tasks, we focus on developing a novel directional sensing technology. Since mobile robots can move in any direction to carry out the mission, the technology should ensure accurate direction-finding capabilities. Furthermore, from the viewpoint of mobility, the two most important considerations may include the simplicity and generality of hardware configurations. Along these lines, this paper addresses how to design and realize an efficient DoA estimation method, enabling mobile robots to accomplish the target-oriented missions.

Our development approach includes the following two aspects. First, robots continue to move toward a target until their task is finished. Therefore, their navigation performance should be improved in a dynamic unstructured environment through an effective, efficient, and accurate direction finding system. For this, a new phase difference based estimation model is proposed, where the incidence angles from an electromagnetic emitter are not always identical with each other. Secondly, when the estimation model is implemented in either the hardware or software, it is desirable to reduce additional devices and units as much as possible. It is often the case that small and low-cost mobile robots with limited power or computational resources are preferable in many cases. Ultimately, our prototype installed on a robot is characterized by simplicity and generality, as well as the capability for ensuring accuracy. To this end, a new DoA detection prototype based on the proposed estimation model is devised and realized.

## II. Phase Difference Based Estimation Model

### A. Model Definition

First of all, we introduce definitions and notations frequently used in this paper. As depicted in Fig. 1, we consider that two antennas, denoted by $A_1$ and $A_2$, are mounted on

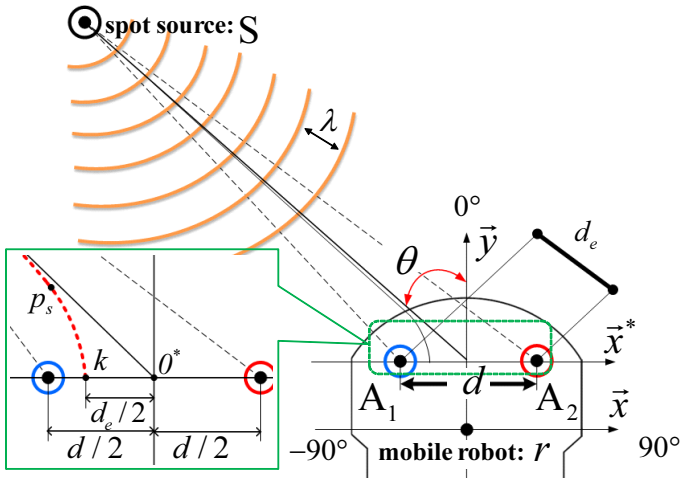


Fig. 1. Definitions and notations for a DoA approximation model

top of a mobile robot $r$. An electromagnetic source $S$ emits electromagnetic radiation at a frequency $f$ (or wavelength $\lambda$). Specifically, $S$ is regarded as a spot source. At a time $t$, electromagnetic signals (for simplicity, signals, afterwards) received at $A_1$ and $A_2$ are defined as $e_1(t)$ and $e_2(t)$, respectively. Next, $r$ has its local coordinates $\vec{x}$ and $\vec{y}$, where $\vec{y}$ defines the vertical axis of $r$'s coordinates as its heading direction. Separately, for DoA computation, the directions of $\vec{y}$ and $\pm\,\vec{x}$ are specified as 0-degree and $\pm$ 90-degree directions, respectively.

In Fig. 1, the locations of $A_1$, $A_2$, and $S$ are denoted by $p_{a1} = (x_{a1}, y_{a1})$, $p_{a2} = (x_{a2}, y_{a2})$, and $p_s = (x_s, y_s)$, respectively. The distance between two arbitrary points $p_i$ and $p_j$ is expressed as $dist(p_i, p_j)$. Specifically, $dist(p_{a1}, p_{a2})$ is defined as $d$ where $\vec{y}$ bisects $d$. Moreover, we consider electrical traveling distances of signal propagation to $p_{a1}$ and $p_{a2}$ from $p_s$. The difference between the traveling distances caused by $d$ is formally named the electrical distance, denoted by $d_e$.

### B. Estimation Model

When $S$ is assumed to be a flat surface source, the angle of incidence at which $e_1(t)$ and $e_2(t)$ arrive at $A_1$ and $A_2$ are equiangular. Then, the arrival angle $\theta$ can be easily obtained through trigonometry such as the law of cosines, since the phase difference $\phi_{12}$ is directly related to the angle of incidence. However, it would be difficult to find plane waves in real propagation environments, particularly when the signals are relatively long in wavelength and low in frequency.

If a spot source is assumed, the incident angles are not always identical to each other. Considering various applications of mobile robots, it is desirable to improve the accuracy of $\theta$ estimation. Ultimately, we aim at developing a computationally-efficient model based on the spot source, enabling mobile robots to obtain $\theta$ as accurately as possible. Moreover, it is considered preferable not to measure the angles with additional hardware option and/or data, keeping the hardware architecture simple.

The idea behind the method of $\theta$ estimation is to use $d_e$ as another representation of the phase difference $\phi_{12}$, as will hereinafter be explained. The electrical traveling distances from $p_s$ to $p_{a1}$ and $p_{a2}$, respectively, can be described as follows:

$$\begin{aligned} dist(p_{a1}, p_s) &= |\overline{p_{a1}p_s}| = \sqrt{(x_{a1}-x_s)^2 + (y_{a1}-y_s)^2} \\ dist(p_{a2}, p_s) &= |\overline{p_{a2}p_s}| = \sqrt{(x_{a2}-x_s)^2 + (y_{a2}-y_s)^2} \end{aligned}, \quad (1)$$

and $d_e$ is given by

$$d_e = |\overline{p_{a1}p_s} - \overline{p_{a2}p_s}|. \quad (2)$$

Now, $\phi_{12}$ is obtained by multiplying $d_e$ by $\frac{360}{\lambda}$.

$$\phi_{12} = \frac{360}{\lambda} d_e. \quad (3)$$

(3) can be rewritten as

$$d_e = \frac{\lambda}{360} \phi_{12}. \quad (4)$$

Using (2) and (4), the geometric relationship between $d_e$ and $\phi_{12}$ can be summarized by the following equation.

$$d_e = |\overline{p_{a1}p_s} - \overline{p_{a2}p_s}| = \frac{\lambda}{360} \phi_{12}. \quad (5)$$

From the configuration of $A_1$ and $A_2$, (5) can be used to find one candidate location for $p_s$. Due to the unknown $\phi_{12}$, there still exist numerous candidates for $p_s$. This means that $\theta$ varies according to the candidates.

Next, we explain how (5) can be used to estimate $\theta$. The solution trajectories of (2) for $p_s$ bring up the image of curves due to a quadratic equation. Moreover, $p_s$ on the curves should satisfy the condition that the distance difference between $|\overline{p_{a1}p_s}|$ and $|\overline{p_{a2}p_s}|$ is equal to $d_e$. For the sake of simplicity, as depicted in Fig. 1, the $\vec{x}$-axis is translated along the $\vec{y}$-axis so that it (the $\vec{x}^*$-axis in the figure) passes through $p_{a1}$ and $p_{a2}$. By doing this, (5) can be simplified to

$$\sqrt{(x_{a1}-x_s)^2 + y_s^2} - \sqrt{(x_{a2}-x_s)^2 + y_s^2} = d_e, \quad (6)$$

where $y_{a1}$ and $y_{a2}$ turn out to be zero. Since $\vec{y}$ bisects $d$, $|x_{a1}|$ and $|x_{a2}|$ are equidistant from $0^*$ (the origin of the $\vec{x}^*$- and $\vec{y}$-axes). Substituting $-x_{a1}$ for $x_{a2}$ in (6), and then rearranging and squaring both sides of the equation, we obtain the following equation.

$$(x_{a1}^2 - k^2)x_s^2 - k^2 y_s^2 = k^2(x_{a1}^2 - k^2), \quad (7)$$

where $k$ indicates $\frac{d_e}{2}$. After dividing both sides by $k^2(x_{a1}^2 - k^2)$, (7) is rewritten as

$$\frac{x_s^2}{k^2} - \frac{y_s^2}{(x_{a1}^2 - k^2)} = 1. \quad (8)$$

Intuitively, we know that (8) is the representation of a hyperbola whose two focal points are $p_{a1} = (x_{a1}, 0)$ and $p_{a2} = (-x_{a1}, 0)$. Generally, a hyperbola is defined as the locus of all points such that the difference between the distances to two focal points from a given $p_s$ is equal to $2|x_{a1}|$. Furthermore, the distance from $0^*$ to either vertex is equivalent to $k$. Defining another variable $m = \sqrt{x_{a1}^2 - k^2}$, (8) in the simple form is written:

$$\frac{x_s^2}{k^2} - \frac{y_s^2}{m^2} = 1, \quad (9)$$

where the asymptotes of (9) are obtained: $y_s = \pm\frac{m}{k} x_s$.

Using the geometric analogy between the hyperbola and (8) with $p_{a1}$ and $p_{a2}$ as the two focal points, $\frac{d}{2}$ and $\frac{d_e}{2}$ are substituted for $|x_{a1}^2|$ and $k$, respectively. Since $\theta$ is defined starting from $\vec{y}$ in Fig. 1, $\theta$ is given:

$$|\theta| = \tan^{-1}\frac{\frac{d_e}{2}}{\sqrt{(\frac{d}{2})^2-(\frac{d_e}{2})^2}} = \tan^{-1}\frac{d_e}{\sqrt{d^2-d_e^2}}, \quad (10)$$

where $d > d_e$. Formally, (10) is defined as the DoA estimation model. For convenience, the slope $\eta$ is substituted:

$$\eta = \pm\frac{d_e}{\sqrt{d^2-d_e^2}}. \quad (11)$$

Finally, the asymptotes with respect to $\vec{x}^*$ and $\vec{y}$ are represented:

$$y_s = \pm\frac{1}{\eta}x_s. \quad (12)$$

### C. Discussions

Here we further discuss the characteristics of the proposed model. First, although the asymptotes in (12) are straight lines passing through $0^*$, $\eta$ depends on $d_e$. In other words, the asymptotes vary according to $d_e$, which means that $\theta$ can be estimated efficiently and accurately based on $\eta$.

Secondly, in comparison with $\phi_{12}$ ($= \frac{360}{\lambda}d_e$ in (3)), the phase difference in most existing works is defined as $\frac{360}{\lambda}d\cos\alpha$, where $\alpha$ is the same incident angle. Considering mobile robot applications, the error between $\theta$ and $\alpha$ can directly affect the performance and efficiency. More interestingly, in (10), $\theta$ becomes 0 as $d_e$ approaches zero, indicating that $S$ is located in the 0-degree direction, namely the $r$'s heading direction. The 0-degree direction will help a mobile robot maintain its relative direction as a virtual signpost.

Thirdly, (10) can not determine whether $\theta$ is positive or negative due to the limited number of antenna array elements with $A_1$ and $A_2$. The alternative is to enlarge the number of antennas. But, the more of antennas there are, the more complicated the organization and integration of mobile robots might be. Instead of adding additional antenna elements, a simple hardware unit is devised to obtain an accurate $\theta$. A detailed description will follow in Section III.

## III. Implementation of DoA Detection Prototype

This section explains how to realize a DoA detection prototype based on the proposed estimation model. Moreover, this prototype is integrated into our commercially available mobile robot platform to examine whether it is suitable for mobile robot target tracking.

### A. Design Considerations for DoA Detection Prototype

The design and implementation of our DoA detection prototype aims to explore the possibility of widespread utilization of the mobile robot applications mentioned in Section I. To this end, our design considers "simplicity" the most important features, requiring neither sophisticated equipments for signal detection (e.g., global timer, directional antenna and actuator) nor high-performance computation devices. Ultimately, the simple prototype can be easily integrated into a wide range of mobile robot platforms.

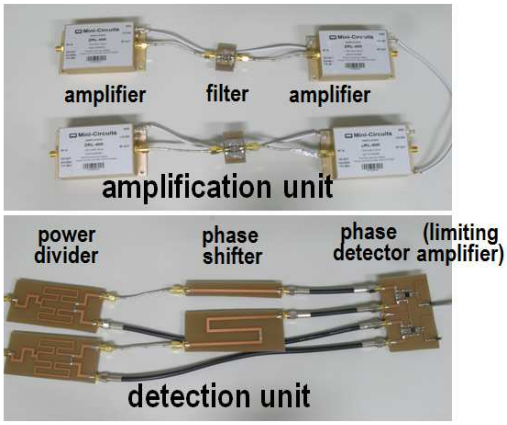


(a) hardware configuration

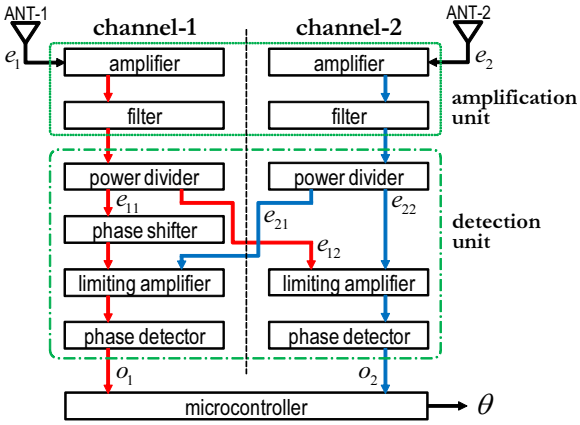


(b) schematic signal flow

Fig. 2. DoA detection prototype and schematic signal flow

Meanwhile, the prototype is required to provide sufficient accuracy for $\theta$ measurements based on the proposed estimation model, since mobile robots can move in any direction. Specifically, to enhance direction finding accuracy, several hardware units are newly designed that control input signals received at each antenna. The units allow the prototype to utilize the signals effectively regardless of whether the robot moves instantaneously.

When we choose a waveband suited for the potential applications, there are several criteria that should be considered, such as waveband density, data management, and reliability. Based on the criteria, the $315MHz$ frequency band is tactically determined in our prototype design. One notable advantage is that it allows the robot to find directions and/or distances while communicating at the maximum $100kbps$. Next, the frequency is less congested than the unlimited industrial, scientific and medical radio bands, resulting in less radio interference. Moreover, longer wavelengths yield longer range, and are better able to carry data through obstacles such as walls and furniture. Practically, Asada and Okamoto reported a radio beacon buried under snow at a depth of $60cm$ could be radiolocated by using triangulation [12].

### B. Prototype Architecture and Component Development

Fig. 2-(a) illustrates the hardware configuration of the DoA detection prototype. The prototype largely consists of

the amplification and the detection units. The amplification unit amplifies and filters received signals. On the other hand, the detection unit plays a role in extracting both the magnitude and the sign of $\theta$ from the signals. For all components, a $50\Omega$ standard has been designed as the characteristic impedance of most commonly available radio frequency (RF) components. Specifically, according to the provisions of Radio Act in Japan, the frequency outputs are set within $500\mu V/m$ at a distance of $3m$.

To begin, the amplification unit including two dipole antennas with $\lambda/4$ in length is composed of four Mini-Circuits ZRL-400 amplifiers and two EPCOS SAW filters. Due to extremely low-power inputs, the amplifiers are configured as two stages. Moveover, $d$ is set as $\lambda/2$.

Next, the detection unit is largely classified into three boards. First, the role of the power divider board is isolation between output channels while maintaining the impedance-matched condition on input and output channels. To minimize the loss of RF signals, a type of the Wilkinson power divider [13] is designed and fabricated as transmission lines on printed circuit boards (PCB). By using the power divider, RF inputs at $A_1$ and $A_2$ are split into two pairs of outputs with the minimum loss. Secondly, the phase shifter board is used to change the transmission phase angle of signals. Using the different lengths of each transmission line on PCBs, the phase shifter is realized, allowing the generation of the 90-degree phase difference between output signals. Thirdly, after the outputs of the phase shifter are synthesized, the phase detector board produces voltage outputs as the sign and the magnitude of $\theta$. Practically, to gain a high-speed phase detection, the mixer-based phase detector is fabricated by integrating an Analog Devices AD8302 chip and passive parts.

As depicted in Fig. 2-(b), individual paths for $e_1$ and $e_2$ are called CHANNEL-1 and CHANNEL-2, respectively. In the amplification unit, $e_1$ and $e_2$ are amplified and filtered. Next, by the power divider, $e_1$ (and $e_2$) are split into $e_{11}$ and $e_{12}$ (and $e_{21}$ and $e_{22}$). Then, $e_{21}$ and $e_{12}$ are mutually exchanged into CHANNEL-1 and CHANNEL-2. After passing through the phase shifter, $e_{11}$'s transmission phase angle is delayed by 90 degrees. In the limiting amplifier, $e_{11}$ and $e_{21}$ ($e_{12}$ and $e_{22}$) are synthesized in CHANNEL-1 (CHANNEL-2) while controlling their magnitudes. By the phase detector, CHANNEL-1 finally outputs either a plus or minus sign with respect to $\vec{y}$. On the other hand, the output of CHANNEL-2 produces the absolute angle with respect to $\vec{y}$.

Fig. 3-(a) shows our robot system integrated with the DoA detection prototype. The overall system largely consists of the following three parts: a commercial MobileRobots Pioneer 3-DX mobile robot including its main controller, the detection prototype, and the microcontroller. A built-in Faraday cage houses the prototype on top of the robot that is used for the cradle of the main controller and the microcontroller. A laptop PC running Microsoft's Windows 7 is used as the main controller, and is placed on the housing. In Fig. 3-(b), the voltage outputs, representing $|\theta|$ and either $+$ or $-$, are fed to the Atmel ATmega128 microcontroller, and converted to 10-bit digital values, leading to a signed value $\theta$. The main controller is linked to the microcontroller and to the robot through RS-232C. Inputs to the main controller include digitalized $\theta$ data.

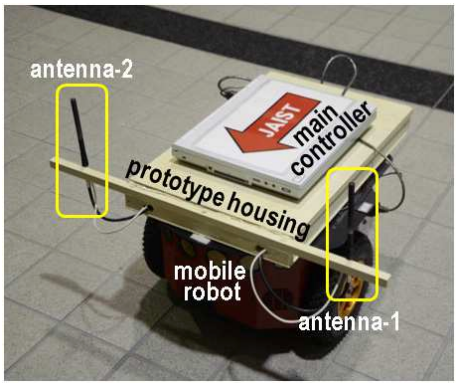


(a) mobile robot integration

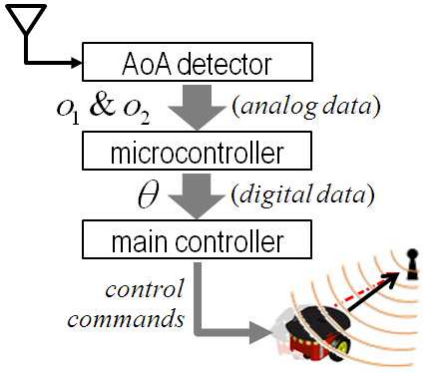


(b) overall control architecture

Fig. 3. DoA detection prototype mounted on a mobile robot

Specifically, the main controller forwards control commands to the robot according to $\theta$.

The outstanding features of the DoA detection prototype are described as follows. Eliminating the use of a sampling frequency and iterative routines, the prototype allows the robot to detect $\theta$ in real time without high-performance computation devices. The use of dipole antennas does not require both a specific device (e.g., directional antennas and their rotation devices) and a sophisticated skill such antenna matching. In addition to these features, the prototype provides us sufficient accuracy for real environment applications. The results for the performance will follow in Section IV.

## IV. EVALUATION RESULTS

When our detection prototype is used as the direction sensing system for mobile robot navigation, it would be essential that the estimate accuracy of $\theta$ be maintained as high as possible. Thus, our evaluation criterion and performance index were designed to examine the extent to which the prototype can minimize the difference between the direction of $S$ and $\theta$. In detail, the first experiments present measurement results to examine whether the prototype works according to desired criteria. Secondly, mobile robot experiments were conducted to verify the performance and the feasibility of the DoA detection prototype.

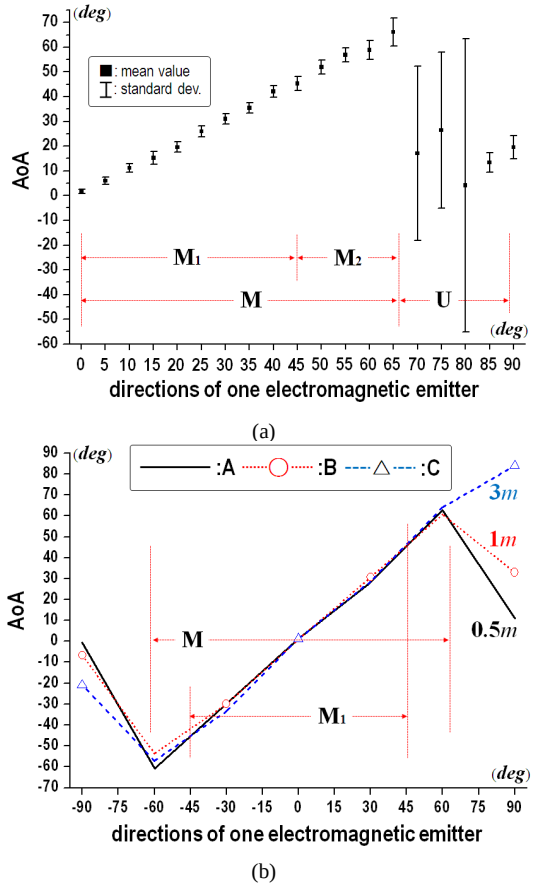


Fig. 4. Statistical analysis of 100 measurements of $\theta$ ((a) according to the interval of 5 degrees while an electromagnetic emitter is located $1m$ away, (b) according to the distance to one electromagnetic emitter while it moves at intervals of 15 degrees

### *A. Mobile Robot Experiments Equipped with DoA Detection Prototype*

This part presents the results of experiments to evaluate the features and performances of the DoA detection prototype and then to investigate its utilization possibility toward mobile robot target tracking. The detailed experimental conditions are summarized as follows. As $S$, an Agilent Technologies E4430B RF signal generator was used according to the legal provisions of Radio Act in Japan. Specifically, to realize a moving $S$, an in-house built J-P RFID tag with the RF carrier frequency $315MHz$ [15] was mounted on top of the mobile robot. The robot moves under the maximum linear velocity of $0.5m/s$ throughout all experiments. The maximum magnitude of the angular velocity is $0.785rad/s$. Two standard Linx Technologies $\lambda/4$ dipole antennas with a gain of $2.14dBi$ were installed at the front of the robot (see Fig. 3-(a)). Finally, our experiments were executed in a large hall.

Fig. 4 shows the results of our statistical analysis, where 100 measurements of $\theta$ were made. The mean values and the standard deviations were represented as the black rectangles and the error bars of the range of 5% to 95% confidence intervals, respectively. First, Fig. 4-(a) plots measurement results according to the interval of 5 degrees while $S$ is kept at $1m$ away from $0^*$. From the results, the test range from 0 to 90 degrees can be classified into two ranges based on the measurability of $\theta$. Within the $M$ range, the mean values of $\theta$ correspond to the assigned directions of $S$. On the contrary, the $U$ range was substantially different from the assigned directions. Moreover, the $M$ range is further divided into $M_1$ and $M_2$ subranges depending on the reliability of $\theta$. The $M_1$ subrange goes from 0 to 45 degrees, where individual standard deviations are less than 2.5 degrees. In the $M_2$ subrange, the standard deviations increase as the acute angles gradually increase from the 0-degree direction. From $S$ located at the distance of $1m$, the means (and the standard deviation) for the 0-degree, 30-degree, and 60-degree directions are 1.75 (0.84), 31.00 (2.12), and 58.8 degrees (3.78), respectively. Although the accuracy in the $M_2$ subrange was debased, $\theta$ could be determined approximately. Based on the statistical analysis of $\theta$ measurements, the $M$ range can be also regarded as a permissible range.

Secondly, Fig. 4-(b) plots the $\theta$ measurement according to assigned distances to $S$ while moving at the interval of 15 degrees. The $A$, $B$, and $C$ lines indicate the mean values measured at $0.5m$, $1m$, and $3m$, respectively. The results displayed that the DoA detection prototype was able to measure $\theta$ from -60 degrees to 60 degrees within the legal provisions of Radio Act. Similar to the results in Fig. 4-(a), we confirmed that the range from about -60 degrees to 60 degrees can be thought of as the permissible range, denoted by $M$. The range from -45 degrees to 45 degrees is formally defined as $M_1$. Specifically, the relationship between $\theta$ and the $S$ direction is linear within $M_1$. This property helps the robot localize a target while moving toward an assigned direction.

Thirdly, to investigate the navigation feasibility of autonomous mobile robot integrated with our DoA detection prototype, path tracking experiments were evaluated. The J-P RFID tag was installed on top of a leader robot (denoted by 'L-Robot'). When L-Robot moves clockwise along an assigned path (see Fig. 5-(a)), a follower robot (denoted by 'F-Robot') equipped with the prototype monitors the direction of L-Robot and computes relative angle differences with respect to the F-Robot's coordinates. Based on the computation, F-Robot tries to follow L-Robot while maintaining its 0-degree direction described in Section II. Fig. 5-(b) shows snapshots for experiments performed under the conditions. In Fig. 5-(c), the red dashed line ('$A$'), the blue dotted line ('$B$'), and the black solid line ('$C$') represent the assigned path, the L-Robot's trajectories, and the F-Robot's trajectories, respectively. From the trajectories, F-Robot could successfully track L-Robot by simultaneously measuring the directions using the DoA detection prototype. Specifically, F-Robot could realize accurate rotations at individual corners. From these results, we confirmed that F-Robot could generate the 0-degree direction navigation motions based on the output of the prototype under our laboratory conditions.

Consequently, the prototype based on the proposed estimation model and its mobile robot integration could provide a good combination measurement capability from the system integration point of view. In general, the phase difference technique works quite well for high SNR but might fail for strong co-channel interference and/or multiple paths. Our future work is devoted to exploring new technological solutions for coping with these limitations.

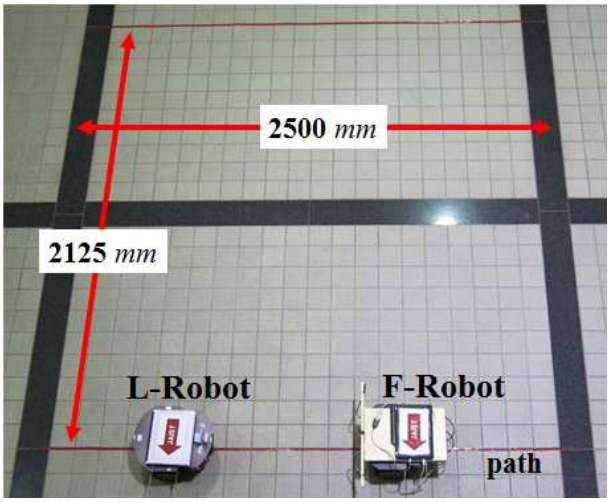


(a) experimental settings

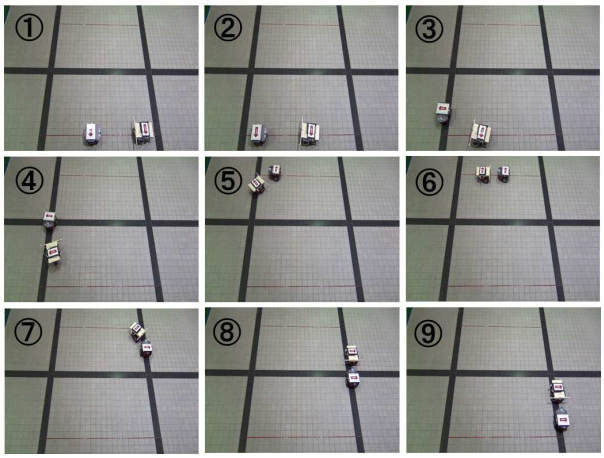


(b) experimental scenes

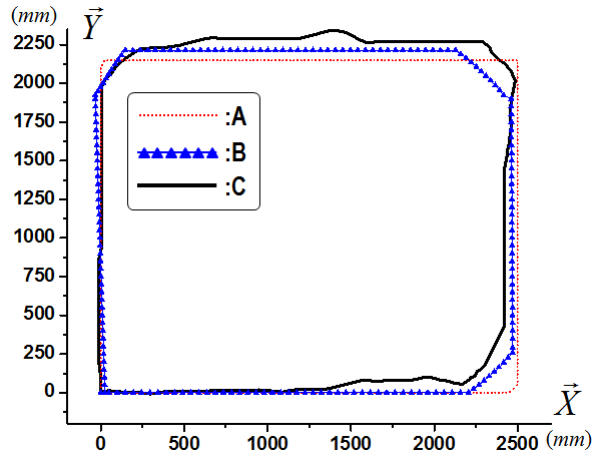


(c) robot trajectories

Fig. 5. Path tracking experiments for the mobile robot equipped with the DoA detection prototype

## V. Conclusion

This paper described a novel method of DoA estimation of electromagnetic signals and its hardware implementation toward mobile robot target acquisition and tracking. Specifically, the hardware-assisted phase difference based estimation model was proposed in order to provide mobile robots with the sufficient direction finding capability. Based on the proposed model, we developed a DoA detection prototype yielding the direction to a fixed or moving electromagnetic source. The hardware prototype was integrated into a commercial mobile robot platform to demonstrate automatic target tracking. Extensive real robot experiments were performed to show the validity of the proposed estimation model. The proposed system can ensure simple configuration, high reliability, and easy integratability into commercial mobile robots. Finally, the DoA detection prototype can facilitate a wide variety of mobile robot missions in a cost-effective way.

## References

[1] M. Malajner, P. Planinsic, and D. Gleich, "Angle of arrival estimation using RSSI and omnidirectional rotatable antennas," *IEEE Sensors Journal*, vol.12, no.6, 1950-1957, 2012.

[2] E. Menegatti, A. Zanella, S. Zilli, F. Zorzi, and E. Pagello, "Range-only SLAM with amobile robot and a wireless sensor networks," *Proc. IEEE Conf. Robotics and Automation*, 814, 2009.

[3] R. Viciana-Abad, R. Marfil, J. M. Perez-Lorenzo, J. P. Bandera, A. Romero-Garces, and P. Reche-Lopez, "Audio-Visual Perception System for a Humanoid Robotic Head," *Sensors*, vol.14, no.6, 9522-9545, 2014.

[4] L.-W. Yeh, M.-H. Hsu, H.-Y. Huang, and Y.-C. Tseng, "Design and implementation of a self-guided indoor robot based on a two-tier localization architecture," *Pervasive and Mobile Computing*, vol.8, no.2, 271-281, 2012.

[5] M. Kim, N.-Y. Chong, and W. Yu, "Robust DOA estimation and target docking for mobile robots," *Intelligent Service Robotics*, vol.2, no.1, 41-51, 2009.

[6] N. B. Priyantha, H. Balakrishnan, E. D. Demaine, and S. Teller, "Mobile-assisted localization in wireless sensor networks," *Proc. 24th IEEE Int. Conf. Computer Communications*, 172–183, 2005.

[7] L. A. Trinh, N. D. Thang, D. Kim, S. Lee, and S. Chang, "Application of matrix pencil algorithm to mobile robot localization using hybrid DOA/TOA estimation," *Int. Journal of Advanced Robotic Systems*, vol.9, 254-263, 2012

[8] B. Xu, G. Sun, R. Yu, and Z. Yang, "High-accuracy TDOA-based localization without time synchronization," *IEEE Trans. Parallel and Distributed Systems*, vol.24, no.8, 1567-1576, 2013.

[9] A. Prorok, L. Gonon, and A. Martinoli, "Online model estimation of ultra-wideband TDOA measurements for mobile robot localization," *Proc. IEEE Conf. Robotics and Automation*, 807-814, 2012.

[10] S. Widodo, T. Shiigi, N. Hayashi, H. Kikuchi, K. Yanagida, Y. Nakatsuchi, Y. Ogawa, and N. Kondo, "Moving object localization using sound-based positioning system with doppler shift compensation," *Robotics*, vol.2, no.2, 36-53, 2013.

[11] P. Chestnut, "Emitter localization accuracy using TDOA and differential doppler," *IEEE Trans. Aerospace and Electronic Systems*, vol.AES-18, no.2, 214-218, 1982.

[12] M. Asada and T. Okada, "Propagation characteristics of beacon radio waves at 400*MHz* on the snow-mounted ground," *Trans. the Institute of Electronics, Information and Communication Engineers-B*, vol.J89-B, no.7, 1318-1324, 2006 (in Japanese)

[13] E. J. Wilkinson, "An N-Way Hybrid Power Divider," *IRE Trans. Microwave Theory Tech.*, Vol.MTT-8, 116-118, 1960.

[14] D. M. Pozar, *Microwave Engineering*, John Wiley & Sons (3rd edt.), 2005.

[15] K. Tatara, G. Lee, H. Ono, and N. Y. Chong, "Locally communicative interaction framework for adaptively self-organizing mobile sensor networks," *Proc. IEEE Int. Conf. Automation Science and Engineering*, 1134-1139, 2012.